New Physics: Sae Mulli,
Vol. 70, No. 1, January 2020, pp. 29∼34
http://dx.doi.org/10.3938/NPSM.70.29

Parametrized Phase Shift Model Analysis for 350 MeV ^{7}Li Elastic Scattering on ^{12}C and ^{28}Si

Yong Joo KIM*
Department of Physics, Jeju National University, Jeju 63243, Korea

(Received 2 September 2019 : accepted 29 October 2019)

The elastic scattering cross sections of 350 MeV ^{7}Li incident on ^{12}C and ^{28}Si target nuclei were analyzed using the parametrized phase shift model. The calculated results reproduced satisfactorily the structures of the angular distribution, and a comparison with experiment gave excellent agreement over the entire angular range. The diffractive oscillatory structures observed in the angular distributions can be understood in terms of the strong interferences between the near-side and the far-side scattering amplitudes while the scattering behavior of a structureless decreasing pattern at large angles is entirely determined by the far-side scattering. The parametrized phase shift was employed to evaluate the optical potential by using the inversion method. The calculated inversion potentials were compared to the Woods-Saxon potentials obtained from an optical model analysis.

PACS numbers: 25.70.−z, 25.55.Ci, 24.10.Ht
Keywords: Parametrized phase-shift model, Inversion potential, Elastic scattering, ^{7}Li + ^{12}C, ^{7}Li + ^{28}Si

I. Introduction

The elastic differential cross section is calculated from a square of scattering amplitude. The important ingredient in characterizing the scattering amplitude is the nuclear phase shift. One of the models used for the analysis of elastic scattering data is the parametrized phase shift model [1], in which the nuclear phase shift is expressed as a parametrized form. Since this model provides an analytic expression for the scattering amplitude, it have been employed [2–6] for many years in the description of nucleus-nucleus elastic scattering at low and intermediate energies. Until now, several forms for parametrized phase shift model are known [1]. The parametrized phase shift model based on McIntyre parametrization [7] involves five parameters for a nuclear phase shift, and actually proved to give good fits to the elastic scattering data. The phase shift parameters in this model can be extracted by fitting the elastic scattering data and provide information on scattering properties such as the strong absorption radius and rainbow phenomenon, etc. Throughout this paper, we will use the phase shift model based on McIntyre parametrization to analyze the elastic scattering data and call it simply "parametrized phase shift model (PPSM)".

In parallel with the elastic differential cross section, the knowledge of the nuclear potential between two colliding nuclei is of fundamental important to investigate the interaction regions which have mainly influences on the elastic cross section. There has been a great deal of study [8–12] to evaluate the inversion potential from parametrized phase shift model. Fayyad *et al.* [8] reported the inversion solution to Woods-Saxon type optical model potential determined from the McIntyre phase shift. The parametrized phase shift model based on Ericson parametrization was employed [9] to analyze the heavy-ion scattering data, and to determine the corresponding optical potential using the Glauber's eikonal approximation. In our previous paper [13], we used the PPSM to analyze the elastic scatterings of α+ ^{58}Ni system at E_{lab} = 288, 340 and 386 MeV, respectively, and evaluated the optical potential using the inversion procedure with the relation of McIntye phase shift and a Woods-Saxon type optical potential.

*E-mail: yjkim@jejunu.ac.kr

The elastic data [14] for ^{7}Li + ^{12}C and ^{7}Li + ^{28}Si systems at 350 MeV have been measured and analyzed using the optical and folding models. The elastic data of these systems have attracted considerable interest because they display two different structures: the forward-angle measurements show diffractive oscillations, and the large-angle ones are characterized by smooth exponential falloff. In this paper, we hope to draw attention towards a PPSM to analyze the elastic scattering of ^{7}Li + ^{12}C and ^{7}Li + ^{28}Si systems at 350 MeV. The purpose of this paper is to understand the elastic differential cross sections of ^{7}Li + ^{12}C and ^{7}Li + ^{28}Si systems at E_{lab} = 350 MeV within the framework of the PPSM. Furthermore, using the phase shift obtained from the present analysis, we calculate the optical potential by the inversion method. The calculated potentials are compared with the the Woods-Saxon potentials obtained in optical model analysis.

II. Theory

The nucleus-nucleus elastic scattering cross section between two nonidentical spin-zero nuclei is defined by the expression

$$\frac{d\sigma}{d\Omega} = |f(\theta)|^2, \tag{1}$$

where the scattering amplitude $f(\theta)$ is given by

$$f(\theta) = f_R(\theta) + \frac{i}{2k}\sum_{L=0}^{\infty}(2L+1)\exp(2i\sigma_L)(1-S_L)P_L(\cos\theta). \tag{2}$$

Here $f_R(\theta)$, k, σ_L and $P_L(\cos\theta)$ are the Rutherford scattering amplitude, the wave number, the Coulomb phase shift and the Legendre polynomial, respectively. The nuclear scattering matrix element S_L is associated with the nuclear phase shift δ_L as follows

$$S_L = \exp[2i\delta(L)] = \exp[2i\{\delta_R(L) + i\delta_I(L)\}]. \tag{3}$$

According to the parametrized phase shift model based on the McIntyre's parametrization [2,7] of the S_L, the real ($\delta_R(L)$) and imaginary ($\delta_I(L)$) parts of nuclear phase shift $\delta(L)$ are given as

$$\delta_R(L) = \mu\left[1+\exp(\frac{L-L'_g}{\Delta'_g})\right]^{-1} \tag{4}$$

and

$$\delta_I(L) = \frac{1}{2}\ln\left[1+\exp(\frac{L_g-L}{\Delta_g})\right]. \tag{5}$$

As Eqs. (4) and (5) show, McIntyre phase shift contains five adjustable parameters : L'_g, L_g, Δ'_g, Δ_g and μ. Here, L'_g and L_g are grazing angular momenta in L-space which are semiclassically related to the interaction radius of the colliding nuclei in real space. The corresponding widths Δ'_g and Δ_g measured the width of transition region in the angular momentum space. With regard to the parameter μ, it is introduced to give the strength of the real nuclear phase shift.

Using the semiclassical relationships : $b = (L+1/2)/k$, $b_0 = (L_g+1/2)/k$, $b'_0 = (L'_g+1/2)/k$, $d = \Delta_g/k$ and $d' = \Delta'_g/k$, the nuclear phase shift given in Eqs. (4) and (5) can further be expressed as :

$$\delta_R(b) = \frac{\mu}{1+\exp[(b-b'_0)/d']} \tag{6}$$

and

$$\delta_I(b) = \frac{1}{2}\ln[1+\exp(\frac{b_0-b}{d})], \tag{7}$$

where b, b_0 and b'_0 are the impact parameters, d and d' are surface diffuseness quantities.

Following the Glauber's eikonal approximation [8,15], the nuclear phase shift $\delta(b)$ is connected with the optical potential $U(r)$ given by

$$\begin{aligned}\delta(b) &= -\frac{k}{2E}\int_b^{\infty}\frac{rU(r)}{\sqrt{r^2-b^2}}dr \\ &= -\frac{k}{2E}\int_b^{\infty}\frac{r(V(r)+iW(r))}{\sqrt{r^2-b^2}}dr.\end{aligned} \tag{8}$$

From above equation, we get

$$\delta_R(b) = -\frac{k}{2E}\int_b^{\infty}\frac{rV(r)}{\sqrt{r^2-b^2}}dr \tag{9}$$

and

$$\delta_I(b) = -\frac{k}{2E}\int_b^{\infty}\frac{rW(r)}{\sqrt{r^2-b^2}}dr. \tag{10}$$

The inverse solutions to these equations are given by

$$V(r) = \frac{4E}{k\pi}\frac{1}{r}\frac{d}{dr}\int_r^{\infty}\frac{\delta_R(b)}{\sqrt{b^2-r^2}}bdb \tag{11}$$

and

$$W(r) = \frac{4E}{k\pi}\frac{1}{r}\frac{d}{dr}\int_r^{\infty}\frac{\delta_I(b)}{\sqrt{b^2-r^2}}bdb. \tag{12}$$

By replacing $b = \sqrt{r^2+u^2}$ and substituting Eqs. (6) and (7) into Eqs. (11) and (12), the inversion potentials can further be expressed as follows :

$$V(r) = -\frac{4E\mu}{k\pi d'}\int_0^\infty \frac{1}{\sqrt{r^2+u^2}}\frac{\exp[(\sqrt{r^2+u^2}-b'_0)/d']}{(1+\exp[(\sqrt{r^2+u^2}-b'_0)/d'])^2}du \quad (13)$$

and

$$W(r) = -\frac{2E}{k\pi d}\int_0^\infty \frac{1}{\sqrt{r^2+u^2}}\frac{1}{1+\exp[(\sqrt{r^2+u^2}-b_0)/d])}du, \quad (14)$$

which can be calculated numerically.

III. Results and Discussion

The parametrized phase shift model has been used to calculate the differential cross sections for 350 MeV ^{7}Li elastic scatterings on ^{12}C and ^{28}Si target nuclei. A spin-orbit effects were not taken into account in the calculations of angular distributions because analyzing power data were not measured, and an insensitivity to this spin-orbit interaction was found in the differential cross sections. We searched five input parameters (L_g, L'_g, Δ_g, Δ'_g, and μ) whose values yield the minimize χ^2/N value for elastic data. The corresponding phase shift parameters are listed in Table 1 together with the χ^2/N values. As shown in this Table, very good χ^2/N values were obtained from the PPSM calculations. It can be noticed in Table 1 that the grazing angular momentum L_g for the imaginary phase shift has higher value compared to one L'_g for real phase shift, and two grazing angular momenta $L'_g s$ increase as the target mass becomes heavier. The solid curves in Fig. 1 show the predictions of the PPSM calculations. The solid circles are the experimental data taken from Ref. [14]. The elastic scattering data are characterized by diffractive oscillations at forward angles and structureless decreasing patterns at the large angles. As Fig. 1 shows, the PPSM calculations reproduced satisfactorily these characteristics of the elastic angular distributions for 350 MeV ^{7}Li on ^{12}C and ^{28}Si. Overall fits to the experimental data are exceedingly good over the whole angular ranges, and good fits are also reflected by χ^2/N values for two scattering systems shown in Table 1. The good agreements between experimental data and PPSM calculations indicate that the PPSM is useful approach in the description of elastic scatterings for ^{7}Li + ^{12}C and ^{7}Li + ^{28}Si systems at 350 MeV.

Table 1. Input values determined from the PPSM analysis for ^{7}Li elastic scattering at 350 MeV, along with the minimum $\chi^2/N-$values

Target	L_g	Δ_g	L'_g	Δ'_g	μ	χ^2/N^a
^{12}C	33.1313	4.0552	23.2739	5.4575	3.758	1.00
^{28}Si	53.2442	8.2816	35.5347	6.9922	4.325	1.88

^{a}10 error bars, $\chi^2/N = (1/N)\sum_{i=1}^{N}\left[\frac{\sigma_{\rm th}(\theta_i)-\sigma_{\rm ex}(\theta_i)}{\Delta\sigma_{\rm ex}(\theta_i)}\right]^2$

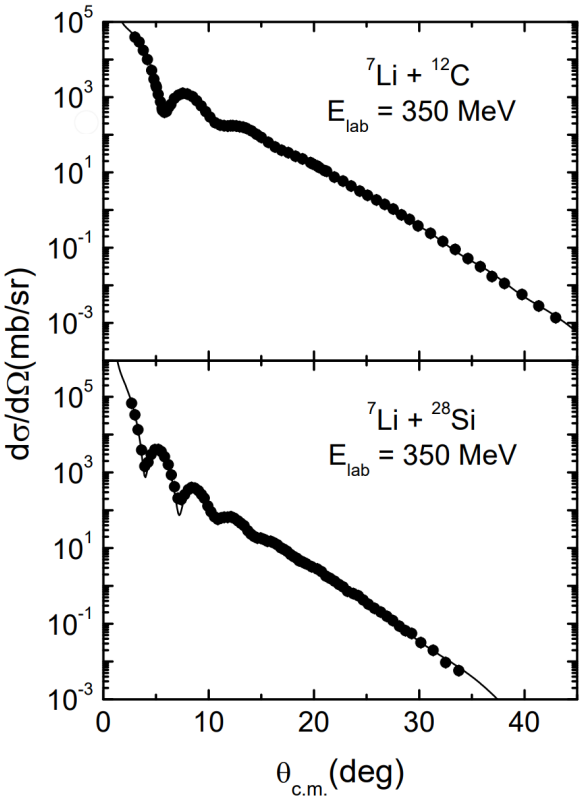

Fig. 1. Elastic scattering angular distributions at 350 MeV for ^{7}Li + ^{12}C and ^{7}Li + ^{28}Si systems fitted by parametrized phase shift model (solid curves). Experimental data [14] are shown as solid circles.

According to the Fuller's formalism [16], the elastic amplitude can be decomposed into the near-side and the far-side components. This formalism was employed to understand the structure of the cross sections for elastic scattering of 350 MeV ^{7}Li on ^{12}C and ^{28}Si. The near-side and the far-side cross sections are displayed as dotted and dashed curves in Fig. 2, while the solid curves denote the differential cross sections shown in Fig. 1. The differential cross section is not just a sum of the near-side and the far-side cross sections, but contains an interference

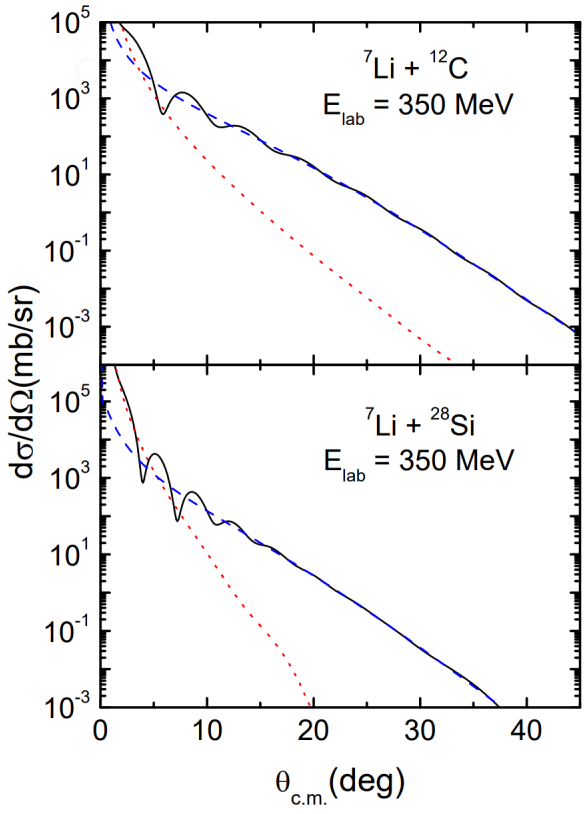

Fig. 2. (Color online) Decomposition of the ^{7}Li + ^{12}C and ^{7}Li + ^{28}Si elastic scattering cross sections (solid curves) at E_{lab} = 350 MeV into the near-side (dotted curves) and the far-side (dashed curves) components using the Fuller's method [16].

between the near- and the far-side amplitudes. The characteristics obtained from near/far decompositions are : (1) the diffractive oscillations in the elastic angular distributions at small angles are attributed to the strong interference between the near-side and the far-side amplitudes, (2) the near-side cross sections are comparable in magnitude with the far-side ones at the crossing angles $\theta_{cross} = 3.60^o$ and 5.30^o (see Table 2 and Fig. 2) for ^{12}C and ^{28}Si target, respectively, indicating that θ_{cross} is found to increase as the target mass becomes heavier, (3) the far-side component plays an important contribution to the large-angle cross sections with smooth exponential falloff behavior.

Table 2 shows the analysis results of PPSM calculation for 350 MeV ^{7}Li elastic scattering on ^{12}C and ^{28}Si target nuclei : crossing angle, the reaction cross section, strong absorption radius and critical angular momentum. The critical angular momentum $L_{1/2}$ is the $L-$value corresponding to $|S_L|^2 = 1/2$. The strong

Table 2. Quantities obtained from the PPSM analysis for ^{7}Li elastic scattering at 350 MeV. All quantities are defined in the text.

Target	^{12}C	^{28}Si
θ_{cross}(deg)	3.60	5.30
$\theta_{c.r.}$(deg)	0.68	1.22
$\theta_{n.r.}$(deg)	-17.75	-14.70
$L_{1/2}$	36.7055	60.5434
$R_s(fm)$	5.499	7.156
σ_{R_s} (mb)	950	1609
σ_R (mb)	980	1677

absorption radius R_s is related to the critical angular momentum $L_{1/2}$ through the formula $R_s = \{\eta + \sqrt{\eta^2 + L_{1/2}(L_{1/2}+1)}\}/k$, where η is the Sommerfeld parameter. In Table 2, σ_{R_s} is the geometrical reaction cross sections defined as $\sigma_{R_s} = \pi R_s^2$ and σ_R is the reaction cross sections obtained from partial wave sums $\sigma_R = (\pi/k^2)\Sigma_{L=0}^{\infty}(2L+1)(1-|S_L|^2)$. Table 2 shows, the values of σ_{R_s} are comparable to the ones of σ_R. The fairly good agreements indicates that the strong absorption radius can give an information on the magnitude of reaction cross section. As expected, the R_s value increases as the target mass becomes heavier, consequently, leading to a larger value of the reaction cross section.

To know the presence of nuclear rainbow, we plotted in Fig. 3 the deflection function versus the angular momentum L. In this figure, the solid curves denote the deflection function given by the analytic formula $\theta_L = 2(d/dL)(\sigma_L + \delta_R(L))$, while the dotted curves are a pure Coulomb deflection function. When the deflection function has a relative maximum or minimum $(d\theta_L/dL = 0)$, the angle at maximum (minimum) is called as Coulomb $\theta_{c.r.}$ (nuclear $\theta_{n.r.}$) rainbow angle. The Coulomb rainbow occurs in a region where the Coulomb potential is large compared to the nuclear one, while the nuclear rainbow arises from the strong nuclear potentials. The deflection function shows a negative nuclear maximum angle at $L \sim 24$ $(L \sim 36)$ followed by a Coulomb rainbow at $L \sim 62$ $(L \sim 80)$ for ^{12}C (^{28}Si) target, which nuclear rainbow is evidently presented in each scattering system. As shown in Fig.3 and Table 2, the deflection function for ^{7}Li + ^{12}C system has a similar structure and provides a somewhat larger magnitude of $\theta_{n.r.}$, in comparison with the results for ^{7}Li + ^{28}Si system.

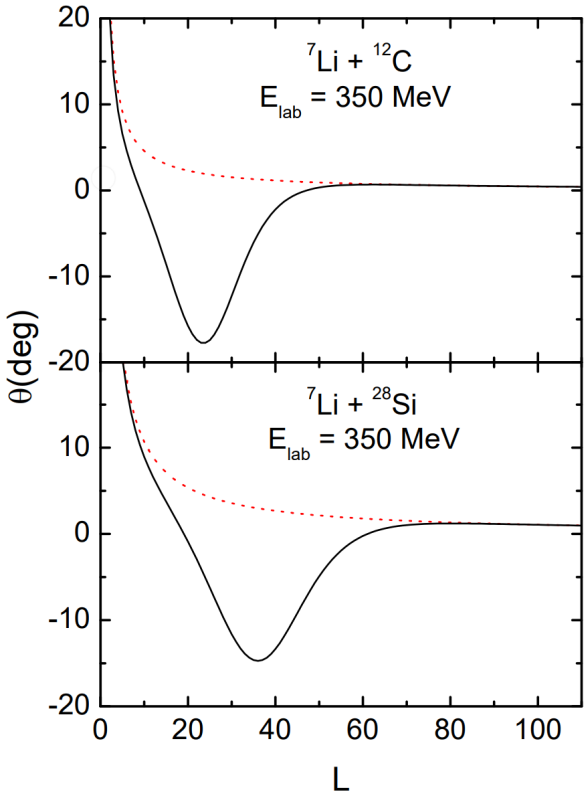

Fig. 3. (Color online) Deflection function (solid curves) determined from the Coulomb and nuclear phase shifts for ^{7}Li + ^{12}C and ^{7}Li + ^{28}Si elastic scatterings at E_{lab} = 350 MeV plotted versus the orbital angular momentum. The dotted curves denote the deflection functions for the Coulomb phase shift.

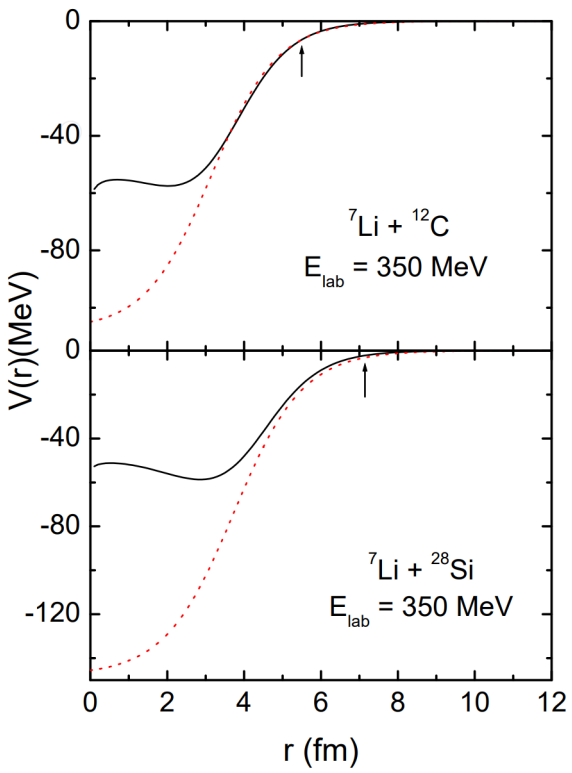

Fig. 4. (Color online) Real part of ^{7}Li + ^{12}C and ^{7}Li + ^{28}Si optical potential at 350 MeV. The dotted and solid curves are the radial shape of Woods-Saxon potential taken from [14] and the inversion potential using Eq. (13), respectively. The arrows denote the position of the strong absorption radius.

Using the phase shift parameters, the calculations of the inversion potentials Eqs. (13) and (14) have been carried out numerically. The results of our calculation are displayed by the solid curves in Figs. 4 and 5. In these figures, the dotted curves denote the Woods-Saxon potentials extracted from the optical model analysis given in Ref. [14]. From a comparison of two curves, we can see the followings : (1) The inversion potentials in this study provide reasonable agreements with the Woods-Saxon ones obtained in optical model analysis near the strong absorption radius, though solid curves for ^{7}Li + ^{28}Si system are slightly different from the dotted curves. This means that the experimental data of 350 MeV ^{7}Li elastic scattering on ^{12}C and ^{28}Si are sensitive to the potential near the strong absorption radius. (2) The real potentials from inversion procedure provided better agreement with the real Woods-Saxon ones obtained in optical model analysis, in comparison with the results of imaginary potentials. (3) Both the real and imaginary parts of the inversion potential differ greatly from those of the Woods-Saxon potential [14] in the interior region. Such big differences between two type optical potentials at small r regions are not important because the measured angular distributions are sensitive mainly to the surface region of the potential.

IV. Concluding Remarks

The elastic scattering data of 350 MeV ^{7}Li incident on ^{12}C and ^{28}Si target nuclei have been analyzed within the framework of parametrized phase shift model. Our calculations have been found to reproduce satisfactorily both of the diffractive oscillations at forward angles and structureless decreasing patterns at large angles appearing on the experimental data for the elastic scattering of ^{7}Li on ^{12}C and ^{28}Si at 350 MeV. The PPSM proved to give

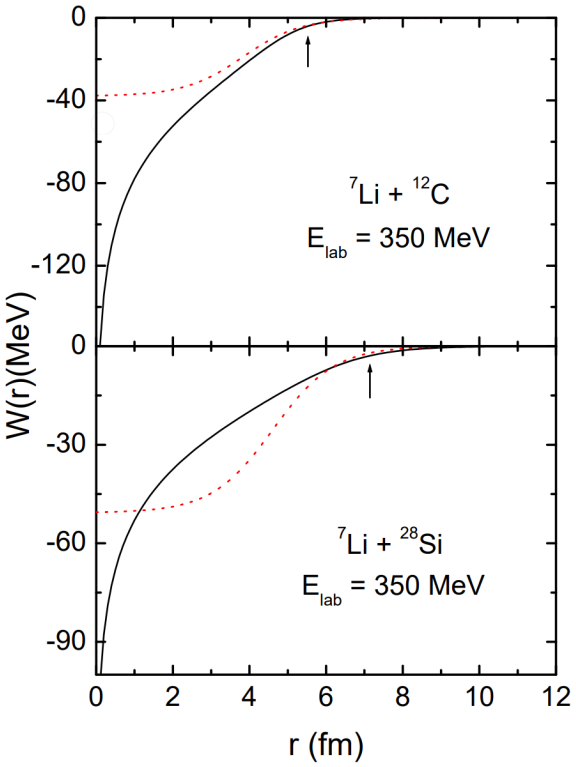

Fig. 5. (Color online) Imaginary part of ^{7}Li + ^{12}C and ^{7}Li + ^{28}Si optical potential at 350 MeV. The dotted and solid curves are the radial shape of Woods-Saxon potential taken from [14] and the inversion potential using Eq. (14), respectively. The arrows denote the position of the strong absorption radius.

good fits to the experimental data over the whole angular range of two scattering systems. Through a near/far decomposition of the differential cross section, the diffractive oscillatory patterns appearing on the forward angular regions are thought to be arose from the strong interference between two scattering amplitudes. However, the structureless decreasing behavior of large angle cross sections is strongly dominated by the far-side scattering. The presence of a nuclear rainbow in each scattering system is apparently evidenced from the deflection function. The magnitude of reaction cross section could be approximately predicted from the strong absorption radius.

Using the inversion procedures that the optical potential can be numerically estimated from the McIntyre phase shift, the inversion potentials were predicted. The inversion potentials of two scattering systems provided reasonable agreements with the Woods-Saxon ones deduced from the optical model analysis in the surface region around R_s, but were found to be greatly different in the interior regions. This facts tell us that most of the contribution to the elastic cross section comes from the surface region.

ACKNOWLEDGEMENTS

This research was supported by the 2019 scientific promotion program funded by Jeju National University.

REFERENCES

[1] D. M. Brink, *Semi-classical methods for nucleus-nucleus scattering* (Cambridge Univ. Press, Cambridge, 1985).
[2] M. C. Mermaz, B. Bonin, M. Buenerd and J. Y. Hostachy, Phys. Rev. C **34**, 1988 (1986).
[3] M. H. Cha and Y. J. Kim, J. Phys. G: Nucl. Part. Phys. **16**, L281 (1990).
[4] S. K. Charagi *et al.*, Phys. Rev. C **48**, 1152 (1993).
[5] M. H. Cha, J. Korean Phys. Soc. **49**, 1389 (2006).
[6] R. I. Badran, H. Badahdah, M. Arafah, and R. Khalidi, Int. J. Mod. Phys. E **19**, 2199 (2010).
[7] J. A. McIntyre, K. H. Wang and L. C. Becker, Phys. Rev. **117**, 1337 (1960).
[8] H. M. Fayyad, T. H. Rihan and A. M. Awin, Phys. Rev. C **53**, 2334 (1996).
[9] N. M. Eldebawi and M. H. Simbel, Phys. Rev. C **53**, 2973 (1996).
[10] Y. J. Kim and M. H. Cha, Int. J. Mod. Phys. E **9**, 299 (2000).
[11] I. Ahmad, M. A. Abdulmomen and G. A. Hamra, Pramana-J. Phys. **65**, 523 (2005).
[12] S. A. Aldenfariya and A. M. Awin, J. Korean Phys. Soc. **64**, 1788 (2014).
[13] Y. J. Kim and S. J. Lee, New Phys. : Sae Mulli, **68**, 55 (2018).
[14] A. Nadasen *et al.*, Phys. Rev. C **52**, 1894 (1995).
[15] A. Vitturi and F. Zardi, Phys. Rev. C **36**, 1404 (1987).
[16] R. C. Fuller, Phys. Rev. C **12**, 1561 (1975).